Earth's Bad Decades: A Sedimentary Record of the Chicxulub Aftermath from the New Jersey Coastal Plain and Offshore

Kenneth G. Miller[1*], Peter J. Sugarman[1], Selen Esmeray-Senlet[2], Alexander Hudak[1], Yoshi Miyazaki[1], W. John Schmelz[1], James V. Browning[1], Timothy Shamus[1,3], Lauren Neitzke Adamo[1], and Richard K. Olsson[1]

1 Department of Earth and Planetary Sciences, Rutgers University, Piscataway, NJ 08854, USA.

2 Chevron Corporation, Houston, TX 77002, USA.

3 Natural Sciences Department, Middlesex College, Edison, NJ 08818, USA.

*** Corresponding author:** Kenneth G. Miller (kgm@rutgers.edu)

ORCID: 0000-0002-7583-7425

This is a non-peer-reviewed preprint submitted to EarthArXiv.

Earth's Bad Decades: A Sedimentary Record of the Chicxulub Aftermath from the New Jersey Coastal Plain and Offshore

Kenneth G. Miller[1], Peter J. Sugarman[1], Selen Esmeray-Senlet[2], Alexander Hudak[1], Yoshi Miyazaki[1], W. John Schmelz[1], James V. Browning[1], Timothy Shamus[1,3], Lauren Neitzke-Adamo[1], Richard K. Olsson[1]
[1] Department of Earth and Planetary Sciences, Rutgers University, Piscataway, NJ 08854, USA.
[2] Chevron Corporation, Houston, Texas, 77002, USA.
[3] Natural Sciences Department, Middlesex College, Edison, NJ, 08818, USA
Corresponding author: K.G. Miller kgm@rutgers.edu, https://orcid.org/0000-0002-7583-7425

ABSTRACT

The New Jersey Coastal Plain (NJCP) preserves records of the Chicxulub impact approximately 2,500 km from the crater, providing a unique archive of ejecta fallout, sediment reworking, ecological disruption, and recovery following the end-Cretaceous mass extinction. Preservation of impact deposits varies with depositional setting. Offshore sections beneath the NJ continental shelf and slope contain major unconformities, likely formed by slope failure and sediment remobilization triggered by the Chicxulub impact and its aftermath. In the NJCP, the most downdip (seaward) site, Bass River (~100 m paleodepth), records an undisturbed spherule layer of rapid fallout of impact ejecta deposited within hours of the event. More updip sites, including Ancora (~70 m paleodepth), contain reworked spherules and deposits consistent with tsunami-related sediment transport. At Campo Pit and the adjacent Buck Pit corehole (~20-30 m paleodepth), a 30-60 cm thick event deposit composed of lower red and upper green clay contains reworked impact spherules, a prominent iridium (Ir) anomaly near the base of the green clay, and several thin white kaolinite laminae near the top of the succession. Grain-size distributions, soft-sediment deformation structures, and reworked spherule-bearing clasts suggest multiple episodes of sediment erosion, transport, and redeposition rather than a single depositional event. The Ir horizon was deposited settling of fine impact-derived particles that followed impact by a decade or more whereas the overlying white laminae may reflect repeated sediment-remobilization events, perhaps associated with impact-triggered aftershocks. At the Inversand core adjacent to Edelman Fossil Park (~30-40 m paleodepth), the Main Fossiliferous Layer (MFL) occurs approximately 50 cm above a bioturbated K/Pg boundary and lacks a significant Ir anomaly, suggesting a complex history of accumulation and reworking. Collectively, these sections may preserve evidence of a decades-long period of post-impact environmental disruption and recovery that we term Earth's "Bad Decades."

INTRODUCTION

The NJCP (**Fig. 1**) preserves one of the most complete records of the Cretaceous-Paleogene (K/Pg) boundary (Olsson, 1960; Olsson et al., 1997, 2002) outside the Gulf of Mexico and provides a unique opportunity to examine both the immediate effects of the Chicxulub impact (Alvarez et al., 1980; Hildebrant et al., 1991) and environmental disruptions that followed. Located approximately 2,500 km from the impact site, the region was in an intermediate position between the devastated Gulf of Mexico and more distal (>5000 km) sites (Schulte et al., 2010); Gulick, 2025). As a result, NJCP strata document a combination of direct ejecta fallout, seismic disturbance, tsunami deposits, ecological collapse, and

early Paleocene recovery. The remarkable preservation of these deposits has made New Jersey a focal region for K/Pg studies for more than 65 years (Olsson, 1960).

The NJCP forms the emergent portion of the Atlantic passive margin and consists of a seaward-thickening wedge of unconsolidated Cretaceous and Cenozoic sediments that dip gently southeastward at ~ 0.6° (~5 m/km). Sediments accumulated on a broad shallow shelf during repeated marine transgressions and regressions, producing a succession of lithologic units bounded by regional unconformities. These unconformity-bounded depositional packages, long recognized as the classic "New Jersey cycles," are now interpreted within a sequence stratigraphic framework as genetically related transgressive-regressive sequences, with lowstand deposits thin or absent in the NJCP. The result is an exceptionally well-preserved archive of changing sea level, paleoenvironments, and sedimentary processes along the western North Atlantic margin (Miller et al., 1998a).

During the Cretaceous, much of New Jersey was submerged beneath a shallow epicontinental sea that graded seaward from shoreface environments to outer shelf (+100 m) settings. Differences in paleowater depth across the shelf exerted a strong control on preservation of the K/Pg boundary. In assigning paleodepths, we use the paleoslope model originated by Olsson (1997) and updated by Esmeray-Senlet et al. (2015). Updip localities such as the Campo and Buck Pits were deposited in upper (<20 m) to lower shoreface (20-30 m) settings, whereas downdip sites such as Ocean Drilling Program (ODP) Leg 174AX Ancora (~70 m) and ODP Bass River (~100 m) sites were located in progressively deeper middle to outer shelf environments. This paleobathymetric gradient provides a natural laboratory for examining how the effects of the Chicxulub impact varied across a continental shelf.

In this study, we integrate observations from the NJCP, focusing on the Campo Pit outcrop and Buck Pit core, with evidence from other onshore and offshore sections to develop a revised interpretation of the K/Pg boundary record. We propose that the boundary deposits preserve not simply the effects of the day of impact, but also a prolonged (decadal) interval of instability characterized by atmospheric fallout, persistent aftershocks, repeated tsunami activity, and sediment remobilization. Viewed in this context, the NJCP records the transition from the catastrophic moments following the Chicxulub impact to a decade-scale period of environmental disruption that may be regarded as Earth's "Bad Decades."

STRATIGRAPHIC SECTIONS

Continental Shelf, Slope, and Deep-sea sections

Early stratigraphic models assumed depositional continuity increased basinward into the deep basin, but chronostratigraphic studies show that deep-water records often contain major hiatuses and erosion from downslope and along-slope processes, reducing rather than increasing stratigraphic completeness (Sloss, 1963; Aubry, 1995). Studies of offshore NJ industry wells found major hiatuses from the Maastrichtian to Paleocene beneath the modern middle and outer continental shelf and upper continental slope (**Fig. 2**), collectively termed the East Coast Sequential Unconformity (Olsson and Wise, 1987). The onshore NJCP and the lower continental slope (Site 605) off NJ contain a record of the K/Pg that is otherwise obliterated across much of the margin (Olsson and Wise, 1987). The cause of this outer shelf and upper slope erosion became clear when studies identified mass failure deposits on the Bermuda Rise, located 700-1200 km offshore in the western North Atlantic, that were triggered by the Chicxulub impact (Norris et al., 2000). As discussed below, the Chicxulub impact generated a primary impact-generated mega-earthquake of Mw 10-11 that caused massive slumping, resulting in the hiatuses (**Fig. 2**).

Bass River, NJ

The ODP Bass River corehole (Miller et al., 1998b) recovered a remarkably complete K/Pg boundary section from the downdip (~100 m paleodepth) Bass River corehole (**Figs. 1, 3**) and identified a 6-cm-thick spherule ejecta layer deposited directly above the boundary (Olsson et al., 1997). The section preserves an abrupt transition from fossil-rich Maastrichtian sediments below the spherule layer to impoverished early Paleocene sediments above, with no evidence of a significant depositional gap. The ejecta bed contains altered impact spherules, shocked quartz, and distinctive impressions at its base

formed when solid spherules settled into soft seafloor mud, indicating rapid fallout from the Chicxulub impact. Impact spherules are submillimeter-sized spherical droplets of impact melt and/or condensates that formed when target rocks were melted and ejected or vaporized during the Chicxulub impact, then cooled and solidified or recondensed while traveling through the atmosphere before settling to the Earth's surface. At the NJCP sites, most original glass spherules have been altered to clay minerals, although their original spherical morphology is commonly preserved. Yancey and Guillemette (2008) suggested that many white carbonate particles in K/Pg boundary deposits in the spherule layer at Bass River are carbonate accretionary lapilli formed from micrometer-sized calcite particles that formed in the leading edge of the Chicxulub impact plume. Their occurrence together with impact glass spherules as far as 2,500 km from the crater indicates that large amounts of carbonate material were vaporized during impact and transported long distances in ejecta clouds, providing evidence for widespread atmospheric dispersal of Chicxulub ejecta consistent with models of a globally spreading dust cloud and vapor plume (Artemieva and Morgan, 2020). Small clay clasts with reworked Cretaceous foraminifera above the ejecta layer were suggested to be reposited by a tsunami or megastorm (Olsson et al., 1997), a topic we explore below. Because the ejecta layer occurs at the extinction horizon and is associated with the sudden disappearance of many Cretaceous planktonic organisms, Olsson et al. (1997) concluded that the Bass River record provides strong evidence that the Chicxulub asteroid impact occurred exactly at the K/Pg boundary and was directly linked to the end-Cretaceous mass extinction.

This undisturbed spherule layer is interpreted as ballistic ejecta that reached the New Jersey shelf within minutes to hours after impact. If the spherules cooled from a ballistic vapor cloud traveling through the atmosphere (Melosh et al., 1990), ejecta would have arrived within ~5–9 minutes; alternatively, if it arrived as an atmospherically transported dust cloud and vapor plume (Artemieva and Morgan, 2020), then it would arrived ~20 minute after impact. The ejecta stratospheric re-entry and associated radiant heating probably occurred 15 minutes to hours after impact as superheated droplets and vapor-condensates fell back through the atmosphere (Melosh et al., 1990). These spherules then settled through the water column in ~1 hour (assuming Stokes settling of 250-micron spherules in 100 m of water) and accumulated on the continental shelf, forming the earliest component of the impact deposit. Thus, the in situ spherule layer represents deposition beginning hours after impact that postdated arrival of P waves in New Jersey (~5–6 min) and arrival of surface waves (~10–20 min), but survived the tsunami wavetrain that arrived 6–8 hours later (Range et al., 2022), reworking the spherules in shallower water locations.

Ancora, Search Farm, Meirs Farms, NJ

Across the New Jersey Coastal Plain, preservation of the impact record varies systematically with depositional setting. Sites updip of Bass River, including Ancora (~70 m paleodepth), contain reworked spherules and sedimentary deposits attributed to tsunami activity (Miller et al., 1999). At the Ancora K/Pg boundary, Hole A contains only a clay-clast layer and no spherule layer, whereas adjacent Hole B (diverted from Hole A and thus decimeters away) contains a distinct though discontinuous spherule layer. In Hole A, clay clasts at the top of the Navesink Formation contain reworked Cretaceous foraminifers indicating redeposition of older Cretaceous material (Miller et al., 1999). In contrast, Hole B preserves two thin layers composed largely of impact-derived spherules mixed with glauconite, clay, and foraminifers. The spherules in Hole B appear to be redeposited rather than in their original position, while their complete absence in Hole A suggests local erosion, nondeposition, or later disturbance of the K/Pg boundary deposits (Miller et al., 1999).

More updip sections at Search Farm and Meirs Farm (**Fig. 3;** paleodepth ~40-50 m) have uppermost Cretaceous dark green glauconite clays (Navesink Formation) overlain by basal Danian light green glauconite clayey sands (Hornerstown Formation). Search Farm and Meirs Farm outcrops and cores (**Fig. 3**) have either a bed of *Cucullaea vulgaris*, a white siderite layer, or a clast of altered impact material (**Fig. 3**). A white bed of altered carbonate (siderite) adjacent to Search Farm (“Boundary Creek”; Wahyudi, 2010) may consist of altered spherules. No spherules were found at either site, but both Search

Farm and Meirs Farm cores yielded modest Ir anomalies of 0.5 ppb (**Fig. 3**) versus 2 ppb at Bass River. Detailed studies of these anomalies suggest that they reflect vertical mixing of the same amount of input found at Bass River that was bioturbated after fallout ~2 years after impact (Esmeray-Senlet et al., 2016).

Campo Pit and Buck Pit Core

Upper Maastrichtian strata exposed at Campo and Buck Pits (**Figs. 4A, 4B**) illustrate the dynamic depositional environments that characterized the latest Cretaceous shoreline. The Shrewsbury Member of the Red Bank Formation, exposed during earlier mining, records a shallowing-upward succession from lower-shoreface hummocky cross-stratified deposits through swaley cross-stratified facies to upper-shoreface planar-bedded sands with common *Thalassinoides* burrows (**Fig. 5**). These deposits represent the upper portion of a Maastrichtian regressive highstand systems tract developed ~1 to 0.3 Myr prior to the terminal Cretaceous events. An unconformity that separates the Red Bank from the overlying Tinton Formation (**Fig. 4**) is associated with a modest (10-20 m) late Maastrichtian (ca. 66.3 Ma) sea-level fall and a subsequent modest transgression across the K/Pg boundary during deposition of the Tinton Formation (Miller et al., 2010; Esmeray-Senlet et al., 2015).

The Campo and Buck Pits provide one of the few exposures of the Tinton Formation that is not completely indurated (**Figs. 4, 6**). It consists of shoreface quartz sands that progressively fine up section and displays increased burrowing as it deepens upward from upper to lower shoreface, capped with a thin ironstone layer (**Fig. 4**). The Tinton Formation elsewhere contains the latest Maastrichtian ammonite *Discoscaphites iris* (Landman et al., 2004) and this 3 m (10 ft) deposit represents the last 0.3 Myr of the Cretaceous. Downdip of the Campo and Buck site, the Tinton Formation consists of indurated muddy quartzose glauconite sands with reworked glauconite that laterally pass into more typical Navesink glauconite muds and sands (**Fig. 7)**.

The K/Pg boundary exposed in the Campo Pit and in the adjacent Buck Pit corehole consists of an event bed(s) comprised of a red and green clay (**Figs. 4, 6, 8**). The section in the Buck Pit corehole (described by Miller et al., 2010; Wahyudi, 2010; Esmeray et al., 2015) consists of the following units from bottom to top:

1) Dark yellowish brown muddy quartz sands are assigned to the Tinton Formation (**Fig. 4**); this represents transgressive deposits of an uppermost Cretaceous-Paleocene sequence that spans the K/Pg boundary (ca. 65.5–66.3 Ma). The sands become progressively muddier and bioturbated up section, reflecting a transgression from the upper (<20 m) to lower shoreface (20-30 m).
2) A thin (1-4 cm-scale) indurated zone with reworked glauconite caps the Tinton here (**Fig. 8**) that is typical of the entire Tinton Formation in other locations. Oxidation and breakdown of weathered glauconite grains (consisting of brown, cracked grains) may have supplied the iron responsible for the red color of the clay and cementation of the underlying Tinton Formation here and elsewhere.
3) A sandy red clay with reworked brown glauconite and clay clasts contains reworked spherules (Esmeray-Senlet, 2015; Esmeray-Senlet et al., 2015). The occurrence of impact spherules within reworked clasts further supports multiple episodes of sediment remobilization rather than a single depositional pulse. The red clay was reported as 7-10 cm thick by E. Rudolf in 1994 (personal communication) and 15 cm thick in a trench in 2014 (**Fig. 4**; Esmeray-Senlet et al., 2015), though we found it to be 28-29 cm in a hand-auger section in 2024 (**Fig. 6**), suggesting lateral variability in thickness that needs further investigation.
4) A 30-cm-thick sandy green clay (Supplementary Material **Fig. S1**) with very coarse-grained lithic fragments contains spherules in the lower part (sample 9; **Figs. 4, 9a**). The first occurrence of the Danian dinocyst *Senoniasphaera inornata* is at the base of this clay (E. Rudolf, personal communication, 1994), and there is an Ir anomaly with a distinct peak at the base of the green clay (**Fig. 6;** Miller et al., 2010).
5) Approximately five to ten thin white laminae occur in the upper green clay (**Fig. 8**). These white layers are highly weathered to kaolinite (Supplementary Material **Fig. S3**), though possible spherules were noted (**Fig. 9b**). The white laminae differ from the enclosing green clay not only

mineralogically, by their enhanced kaolinite content, but also, by the appearance of a distinct clay-sized population absent from the underlying green clay (Supplementary Material **Fig. S2**).

6) Very dark green muddy glauconite sands assigned to the Hornerstown Formation (~12 ft, 3.25 m thick) deposited below storm wave base (much deeper than 30 m).

Our new data for grain-size and lithologic compositional studies (**Fig. 6**) suggest remobilization, likely by tsunamis. The red clay is dominated by degraded, reworked brown glauconite and reworked clasts with spherules; the green clay is dominated by reworked, less degraded light green glauconite that increases upsection and fewer reworked spherules (**Fig. 6**). The overlying Hornerstown Formation had dominant in situ dark green glauconite formed over thousands of years (**Fig. 6**). The green clay displays bimodal grain-size distributions (Supplementary Material **Fig. S2**), with persistent modes near 11 and 83 μm, suggesting deposition from a combination of fine suspended material and a coarser silt/fine sand-sized fraction throughout the interval. An Ir concentration peak occurs at the base of the green clay (**Fig. 6**), marking a distinct horizon deposited a decade or more after impact (Senel et al., 2023; Goderis et al., 2021). At this point, we favor redeposition of spherules by tsunami activity, but we cannot exclude seiche-wave activity. However, seiche deposits are generally found in restricted basins and dominated by fine silts and clays (homogenites; Zafar et al., 2025), whereas tsunamites are generally coarser and multilayered, with normal and inverse grading similar to that in the green clay (**Fig. 6**).

Edelman Fossil Park/Inversand Core

At Edelman Fossil Park (~30-40 m paleodepth), the K/Pg boundary is associated with the contact of the brownish clays of the Navesink Formation with the overlying green burrowed Hornerstown Formation (Fig. 10). As is typical in sections from Tighe Park, Search Farm, and Meirs Farm (**Fig. 3**; Miller et al., 2010), the basal 20-30 cm of the Hornerstown Formation is marked by large (cm-scale) burrows and echinoid fecal pellets (**Fig. 10**). The absence of an Ir anomaly at the highly burrowed Hornerstown/Navesink contact in the Inversand core adjacent to the working Edelman Pit (**Fig. 10**), compared with other NJ locations, suggests removal of the sediments that recorded the Ir fallout (time scale of 1–2 years). The Main Fossiliferous Layer (MFL) contains early Danian fossils of articulated or semi-articulated specimens, including turtles, crocodilians, and bird remains mixed with reworked Cretaceous material (e.g., Obasi et al., 2011; Voegele et al., 2021). The MFL is located about 50 cm above the bioturbated K/Pg boundary in the core (**Fig. 10**). The low Ir anomaly (0.3 ppb) at the MFL suggests reworking of Cretaceous sediments consistent with mixed Cretaceous and Paleocene macrofauna (**Fig. 10**). We suggest that these organisms accumulated shortly after the extinction event and were subsequently buried by aftershock-induced deposits.

Tighe Park

Landman et al. (2007) reported a fossiliferous bed at the top of the Tinton Formation at Tighe Park containing *Pinna laqueata* preserved in life position, the uppermost Cretaceous ammonite *Discoscaphites iris*, and an Ir anomaly at the base of the bed (**Fig. 11**). The disagreement over the *Pinna* bed centers on the relationship between this Ir anomaly and the extinction horizon. Landman et al. (2007) interpreted the Ir anomaly as essentially in situ, implying that the diverse latest Maastrichtian fauna within the Pinna bed survived the Chicxulub impact and thus postdated the Ir fallout. They rejected reworking by tsunamis as an explanation because *P. laqueata* occurs in life position, indicating preservation of an original living community. In contrast, Miller et al. (2010) accepted that the Pinna bed itself is in place and independently verified the presence of the Ir anomaly at the base of the Pinna bed in the Tighe Park core (**Fig. 11**). However, they argued that the Ir anomaly, not the fossil bed, had been displaced downward. By comparison with other New Jersey K/Pg sections (**Fig. 3**), they concluded that impact-derived Ir originally occurred at the extinction horizon and was subsequently mobilized by pore waters, accumulating at a redox boundary at the base of the *Pinna* bed, approximately 20 cm beneath its original stratigraphic position. Under this interpretation, the *Pinna* bed fauna is pre-extinction, and the apparent

separation between the Ir anomaly and the fossil extinction horizon at Tighe Park reflects post-depositional movement of Ir rather than survival of Cretaceous species after impact.

DISCUSSION

The results from the NJCP and offshore sections provide a picture of the intermediate-field response (~1000 to ~5000 km; Schulte et al., 2010) to the Chicxulub impact, with the Campo and Buck site providing key insights into ballistic, airfall, and tsunami activity. The diameter of the Chicxulub crater (~200 km) and the impactor diameter of ~12 km suggest kinetic energy of roughly 10^{23} Joules associated with the impact (Morgan et al., 2022). Typical earthquakes convert ~1% of the released energy into seismic waves, and we therefore estimate that the impact created an initial earthquake with seismic energy of ~10^{21} J, which corresponds to a moment magnitude of Mw ~10-11. This estimate is consistent with other recent estimates of magnitude between Mw ~9.4 and Mw ~11.3 (Bermudez et al., 2025).

The resulting crustal disturbance generated kilometer-scale tsunamis within the Gulf of Mexico (Range et al., 2022) and produced secondary tsunami and swash back waves along the New Jersey margin. Such events would have mixed impact-derived spherules with backwashed coastal-plain sediments, producing the clay-rich deposit preserved at Campo. In contrast, dust and soot remained suspended in the atmosphere for considerably longer periods (~15 years; Senel et al., 2023; Goderis et al., 2021) and was dispersed globally before settling. Recent models suggest that atmospheric residence times for stratospheric Ir is less than 10–20 years (Senel et al., 2023). This prolonged fallout likely produced the Ir concentration peak at the contact at the base of the green clay unit, marking the interval of maximum global settling of impact-derived dust and a time plane approximately 10–20 years after impact. In general, climate models suggest a cocktail of dust, soot, and sulfur led to darkness for at least two years with solar input to the surface returning to normal over 3 or more years (Senel et al., 2023). These models suggest that the impact winter conditions lasted up to 20 years and CO_2-induced global warming of ~5° C initiated just after that and lasted up to several centuries (MacLeod et al., 2025).

Following the initial impact, continued basin adjustment through aftershocks, slope failures, and related tsunami activity likely contributed to deposition of the green clay. A major post-impact seismic event may account for the soft-sediment deformation observed within the red and green clay (**Fig. 8b**). This event is best interpreted as an aftershock because the presence of reworked spherules suggests that it postdated the initial shock, which occurred 10–20 minutes after the impact. The inclusion of the green clay in the deformation suggests that this major aftershock occurred 10-20 years after impact.

Although the Chicxulub impact was not a conventional fault-generated earthquake, our zeroth-order calculations suggest that if crustal adjustment following the impact behaved similarly to large tectonic earthquake sequences, modified Omori-law scaling would predict numerous large aftershocks over the ensuing two decades including several events in the Mw 8 range and dozens in the Mw 7 range (**Fig. 13**). These estimates should be regarded as heuristic rather than predictive because the impact did not generate a typical fault-controlled aftershock sequence. Nevertheless, they suggst that substantial post-impact seismic activity may have persisted for many years and would have repeatedly generated tsunamis and sediment-remobilization events. Such high-energy disturbances may have remobilized unconsolidated shelf sediments, resulting in continued mixing and accumulation within the green clay unit. The persistence of bimodal grain-size distributions in the green clays is consistent with repeated reworking of fine suspended material together with a coarser silt-sized component. Later, less severe, reworking episodes may be recorded by the thin white laminae near the top of the green clay, which we speculate may be individual tsunami deposits formed during episodic sediment disturbance.

Our initial interpretation was that the multiple events recorded by the white layers were redistributed impact spherules that altered to siderite. However, we show that the white layers near the top of the green clay differ from the underlying green clay not only in their grain-size distributions with an enhanced clay-sized mode, but also by the presence of abundant kaolinite clay showing that kaolinite is the source of the white clay (Supplementary Material, **Figs. S2, S3**). Traditionally, kaolinite is viewed as a product of prolonged and intense chemical weathering under warm, humid conditions, commonly

developing over decades to centuries or longer in well-drained tropical soils (e.g., Dill, 2016). However, experimental studies have demonstrated that under biologically active conditions, particularly in the presence of fungi, kaolinite can form on much shorter timescales, ranging from months to years (Pasquale et al., 2024). This observation is particularly relevant given recent evidence for a pronounced fungal spike immediately following the K/Pg boundary (Baker and Casadevall, 2026). These changes are consistent with intensified tropical-subtropical weathering and soil formation, potentially accelerated by prolific fungal activity during the post-impact recovery interval. The shared very-fine-sand population in both the green clay and white layers suggests a common sediment source, whereas the increased clay fraction and kaolinite enrichment in the white layers likely reflect the addition of newly weathered material generated during an interval of intensified post-impact weathering and ecosystem recovery. The white layers may be weathered spherules (an interpretation suggested by possible spherules; **Fig. 8b**) or flaser laminae of heavily weathered coastal plain from numerous waning tsunamis, both of which still fits the bad decades scenario.

Normal marine sedimentation and glauconite formation appear to have resumed on a timescale of decades following the impact. In this interpretation, the red clay records the immediate effects of ejecta fallout, seismic shaking, tsunami deposition, and early post-impact reworking, whereas the overlying green clay records an extended interval of continued sediment remobilization, episodic high-energy events (tsunamis including swash back), and eventual recovery of more typical marine depositional conditions. Based on atmospheric modeling of settling (Senel et al., 2023), the Ir peak near the base of the green clay provides a useful chronostratigraphic marker separating the initial impact-generated deposit (10–20 years) from the subsequent interval of post-impact reworking and environmental recovery (>10–20 years).

We present a chronology (**Fig. 12**) of events on the New Jersey margin that, although speculative, is grounded in observations from the NJCP, particularly the Campo Pit and Buck Pit core. The proposed chronology should be viewed as a working hypothesis rather than a directly dated time scale. During Earth's Bad Day, the sequence of events included the Chicxulub impact, arrival of P waves in New Jersey (~5–6 min), ballistic spherule arrival (~5-40 min), arrival of surface waves (~10–20 min), ejecta re-entry heating (hours), and settling of spherules through the water column (hours). These processes are recorded by the in situ spherule bed at Bass River.

During the first phase of Earth's Bad Decades (0-15 years after impact), atmospheric dust settling, darkness (~3 years), impact-winter conditions (up to 20 years), and repeated large aftershocks likely contributed to deposition of the red clay. Reworked spherules and clay clasts are consistent with repeated episodes of sediment remobilization. At the same time, prolonged darkness (~3 years) and the collapse of primary productivity transformed terrestrial ecosystems. Dead and decaying vegetation accumulated across the dark landscape, creating conditions that favored pronounced fungal proliferation.

During the second phase of Earth's Bad Decade (approximately 15–20+ years after impact), continued sediment remobilization likely by tsunamis was associated with large aftershocks. Evidence for this is provided by reworked spherule-bearing clasts above the Ir horizon (**Fig. 6**), soft-sediment deformation structures, including ball-and-pillow features that include the green clay (**Fig. 8b**), and the series of white laminae in the upper green clay (**Fig. 8a**). Finally, normal shelf sedimentation resumed, marked by deposition of glauconitic sediments in somewhat deeper-water conditions. Water depths during Hornerstown deposition were well below storm wave base (>30 m) and likely ~20 m deeper than decades before. We speculate that this reflects post-impact CO_2 warming (MacLeod, et al., 2025) and sea-level rise due to melting of continental ice sheets or possibly accommodation provided by the effects of earthquakes reactivating local faults or compaction.

FUTURE WORK

The NJCP preserves one of the world's most important records of the Chicxulub impact and its aftermath. Community efforts should focus on protecting these unique archives, and future research

should aim to expand the stratigraphic, sedimentologic, geochemical, and paleontological investigations needed to test the "Earth's Bad Decades" hypothesis proposed here.

A specific priority is the long-term preservation and scientific stewardship of the Campo and Buck Pit as Millstone Geological Park and the Edelman Fossil Park deposits. These localities contain rare and complementary records of the K/Pg boundary and its aftermath that cannot be replaced. The proposed Millstone Geological Park at Campo and Buck Pits will provide an important mechanism for conserving the exceptional boundary exposure, including the impact-related event beds, reworked spherule horizons, Ir-bearing intervals, and putative tsunami laminae. Similarly, continued protection of the Edelman Fossil Park is essential because it preserves an unusual shallow-shelf record of post-extinction ecological recovery and sediment reworking that may be unique along the Atlantic margin.

Future geochemical work should include high-resolution measurements of Ir, platinum-group elements, osmium isotopes, and trace-metal concentrations across the boundary intervals. Such studies could determine the timing of atmospheric fallout relative to the deposition of the event beds and evaluate whether the Campo white laminae contain remobilized extraterrestrial material. Detailed clay mineralogical investigations may also help identify altered impact spherules and distinguish primary fallout deposits from reworked sediments.

Additional coring and high-resolution stratigraphic studies are needed at both the Campo-Buck site and Edelman Fossil Park. New continuously recovered cores would allow detailed sedimentological, ichnological, mineralogical, and geochemical analyses of intervals that are inaccessible, incompletely exposed, or weathered in outcrop. Closely spaced sampling through the red clay, green clay, and white laminae could determine whether the individual layers represent discrete tsunami, seiche, or sediment-gravity-flow events.

Future modeling is also needed to determine the nature of the sedimentary disturbances recorded in the NJCP and to distinguish among seiche, tsunami, and swash-back mechanisms under a range of impact-generated aftershock scenarios. Coupled hydrodynamic and sediment transport models should be employed to evaluate the characteristics of the Atlantic waves that may have been generated by repeated large aftershocks and how these events would have affected sediment erosion, transport, and redeposition in shallow-shelf environments. Such modeling could provide quantitative tests of the origin of the Campo-Buck white laminae, the reworked spherule horizons, and the MFL at Edelman Fossil Park, thereby helping to refine the chronology and processes responsible for Earth's prolonged post-impact "Bad Decades."

ACKNOWLEDGEMENTS

This work began with NJCP studies by R. Olsson in the 1950s, with P. Sugarman introducing us to the Campo Pit in 1992. We thank the Campo and Buck families for providing access to their respective sites. Their generosity has not only enabled the research described here but has also created unique educational and research opportunities for numerous undergraduate and graduate students over the past three decades from universities throughout the region (Rutgers, Rowan, Lehigh, Penn State, and Montclair). The site has served as an outdoor classroom and research laboratory where students have gained firsthand experience in sedimentology, stratigraphy, paleontology, geochemistry, drilling operations, and field mapping. Countless field trips have introduced students, educators, and visiting scientists from around the world to the remarkable geological record preserved at Campo and Buck Pits

Drilling of the NJCP sections was conducted by the U.S. Geological Survey drilling team, particularly G. Cobbs III and J. Gray, both of whom we lost too early. We acknowledge the contributions of numerous Rutgers students, staff, and collaborators who assisted with fieldwork, core description, sampling, laboratory analyses, and curation of the Rutgers Core Repository. The NJCP Drilling Project has provided training opportunities for generations of students and has served as a foundation for interdisciplinary studies of sea-level change, stratigraphy, paleoceanography, and the Cretaceous-Paleogene boundary.

We are especially grateful to those leading efforts to preserve the remarkable K/Pg boundary successions at Campo and Buck Pits, including the Monmouth County Park System (A. Spears, Director, and P. Gleitz, Supervisor of Land Preservation and Planning), Millstone Township (K. Abernethy, Township Administrator), Friends of Millstone Township Historic Registered Properties (P. Butch, President), and the Edelman Fossil Park & Museum of Rowan University under the leadership of K. Lacovara. We acknowledge the vision and generosity of Jean and Ric Edelman, whose support for geological and paleontological education has helped ensure the long-term preservation, study, and public access to the former Inversand Pit, now Edelman Fossil Park.

This research was supported by National Science Foundation Grant EAR-0707407 and by grants supporting the Rutgers Core Repository. We particularly thank B. Huber and S. Gulick for comments.

REFERENCES

Aubry, M.-P., 1995, From chronology to stratigraphy: Interpreting the stratigraphic record, in Berggren, W.A., Kent, D.V., Aubry, M.-P., and Hardenbol, J., eds., Geochronology, Time Scales and Global Stratigraphic Correlation: A Unified Temporal Framework for an Historical Geology: SEPM Special Publication 54, p. 213-274.

Artemieva, N., and Morgan, J., 2020, Global K-Pg layer deposited from a dust cloud: *Geophysical Research Letters*, v. 47, no. 6, e2019GL086562, https://doi.org/10.1029/2019GL086562

Baker, R.P., and Casadevall, A., 2026, Fungal proliferation before and after the Cretaceous-Paleogene mass extinction event in North America: Proceedings of the National Academy of Sciences, v. 123, no. 20, e2536899123.

Bermúdez, H.D., et al., 2025, The sedimentological signature of impact spherules and its relation to ejecta transport mechanisms during the Chicxulub asteroid impact (Cretaceous/Paleogene boundary): Journal of South American Earth Sciences, v. 153, 105338.

Dill, H.G., 2016, Kaolin: Soil, rock and ore: From the mineral to the magmatic, sedimentary and metamorphic environments: Earth-Science Reviews, v. 161, p. 16-129, https://doi.org/10.1016/j.earscirev.2016.07.003.

Esmeray-Senlet, S., 2015, The Cretaceous-Paleogene Boundary in the New Jersey Coastal Plain: Sedimentology, Geochemistry, and Sequence Stratigraphy: Ph.D. dissertation, Rutgers University.

Esmeray-Senlet, S., Özkan-Altıner, S., Altıner, D., and Miller, K.G., 2015, Planktonic foraminiferal biostratigraphy... Journal of Sedimentary Research, v. 85, p. 489-508.

Esmeray-Senlet, S., Miller, K.G., Sherrell, R.M., Senlet, T., Vellekoop, J., and Brinkhuis, H., 2016, Iridium profiles and delivery across the Cretaceous/Paleogene boundary: Earth and Planetary Science Letters, v. 458, p. 75-89.

Gulick, S.P.S., 2025, End of the Cretaceous, in Hart, M.B., et al., eds., Cretaceous Project 200 Volume 1: The Cretaceous World: Geologica Society, London, Special Publications, v. 544, p. 549-570, https://doi.org/10.1144/SP544-2023-176.

Goderis, S., et al., 2021, *Globally distributed iridium layer preserved within the Chicxulub impact structure*: **Science Advances**, v. 7, no. 9, eabe3647, https://doi.org/10.1126/sciadv.abe3647

Hildebrand, A.R., et al., 1991, Chicxulub crater: Geology, v. 19, p. 867-871.

Landman, N.H., Johnson, R.O., and Edwards, L.E., 2004, Cephalopods from the Cretaceous/Tertiary Boundary Interval on the Atlantic Coastal Plain... Bulletin of the American Museum of Natural History, no. 287.

Landman, N.H., Johnson, R.O., Garb, M.P., Edwards, L.E., and Kyte, F.T., 2007, Cephalopods from the Cretaceous/Tertiary boundary interval on the Atlantic Coastal Plain, with a description of the highest ammonite zones in North America. Part 3. Manasquan River Basin, Monmouth County, New Jersey: Bulletin of the American Museum of Natural History, v. 303, p. 1-122, doi:10.1206/0003-0090(2007)303[1:CFTTBI]2.0.CO;2

MacLeod, K.G., Huber, B.T., Tabor, C., Mitra, S., Wheatley, R., Harrison, C., Tessler, M., Bardeen, C., Lovenduski, N.S., Sepúlveda, J., Coupe, J., and Hu, S., 2025, Isotopic evidence from a Brazos River (Texas, USA) Cretaceous/Paleogene boundary section consistent with a pulse of greenhouse warming shortly after the Chicxulub impact: *Global and Planetary Change*, v. 253, article 104924, https://doi.org/10.1016/j.gloplacha.2025.104924

Melosh, H.J., Schneider, N.M., Zahnle, K.J., and Latham, D., 1990, Global firestorm at the Cretaceous-Tertiary boundary: Nature, v. 343, p. 251-254.

Miller, K.G., Sugarman, P.J., Browning, J.V., et al., 1998, Bass River Site: Proceedings of the Ocean Drilling Program, Initial Reports, v. 174AX, p. 1-315.

Miller, K.G., Mountain, G.S., Browning, J.V., et al., 1998, Cenozoic global sea level, sequences, and the New Jersey Transect: Reviews of Geophysics, v. 36, p. 569-601.

Miller, K.G., et al., 1999, Ancora Site studies of the Cretaceous-Paleogene boundary, New Jersey Coastal Plain: ODP Initial Reports 174AX.

Miller, K.G., Sherrell, R.M., Browning, J.V., et al., 2010, Relationship between mass extinction and iridium across the Cretaceous-Paleogene boundary in New Jersey: Geology, v. 38, p. 867-870.

Morgan, J.V., Bralower, T.J., Brugger, J., and Wünnemann, K., 2022, The Chicxulub impact and its environmental consequences: *Nature Reviews Earth & Environment*, v. 3, p. 338-354, https://doi.org/10.1038/s43017-022-00283-y.

Moore, D.M., and Reynolds, R.C., Jr., 1997, X-ray diffraction and the identification and analysis of clay minerals: New York, Oxford University Press, 378 p.

Norris, R.D., Firth, J., Blusztajn, J.S., and Ravizza, G., 2000, Mass failure of the North Atlantic margin triggered by the Cretaceous-Paleogene bolide impact: Geology, v. 28, p. 1119-1122.
Obasi, C.C., et al., 2011, Taphonomy and depositional history of an Upper Cretaceous-Lower Paleogene vertebrate-bearing lag deposit: Journal of Sedimentary Research, v. 81, p. 479-494.
Olsson, R.K., 1960, Foraminifera of latest Cretaceous and earliest Tertiary age in the New Jersey Coastal Plain: Journal of Paleontology, v. 34, p. 1-60.
Olsson, R.K., Miller, K.G., Browning, J.V., Habib, D., and Sugarman, P.J., 1997, Ejecta layer at the Cretaceous-Tertiary boundary, Bass River, New Jersey: Geology, v. 25, p. 759-762.
Olsson, R.K., and Wise, S.W., Jr., 1987, Upper Maastrichtian to Middle Eocene stratigraphy of the New Jersey slope and coastal plain: DSDP 93, p. 1185-1213.
Olsson, R.K., Miller, K.G., Browning, J.V., Wright, J.D., and Cramer, B.S., 2002, Sequence stratigraphy and sea-level change across the Cretaceous-Tertiary boundary on the New Jersey passive margin: GSA Special Paper 356, p. 35-54.
Olsson, R.K., Miller, K.G., and Cramer, B.S., 2002, Collapse and rebuilding of a marine ecosystem across the Cretaceous-Paleogene boundary in New Jersey: GSA Special Paper 356, p. 97-108.
Pasquale, V., Cuadros, J., Dumontet, S., Huertas, F.J., Lettino, A., and Fiore, S., 2024, Kaolinite bioformation at surface conditions: The role of fungi and bacteria: Science of the Total Environment, published online, https://doi.org/10.1016/j.scitotenv.2024.177165.
Poppe, L.J., Paskevich, V.F., Hathaway, J.C., and Blackwood, D.S., 2001, A laboratory manual for X-ray powder diffraction: U.S. Geological Survey Open-File Report 01-041, 88 p.
Range, M.M., et al., 2022, The Chicxulub impact produced a powerful global tsunami: AGU Advances, v. 3, e2022AV000627.
Schulte, P., et al., 2010, The Chicxulub asteroid impact and mass extinction at the Cretaceous-Paleogene boundary: Science, v. 327, p. 1214-1218.
Senel, C.B., et al., 2023, Chicxulub impact winter sustained by fine silicate dust: Nature Geo., v. 16, p. 975-984.
Sloss, L.L., 1963, Sequences in the cratonic interior of North America: Geological Society of America Bulletin, v. 74, p. 93-114.
Smit, J., 1999, The global stratigraphy of the Cretaceous-Tertiary boundary impact ejecta: *Annual Review of Earth and Planetary Sciences*, v. 27, p. 75-113. https://doi.org/10.1146/annurev.earth.27.1.75 [link.springer.com]
Voegele, K.V., et al., 2021, Microstratigraphic analysis of fossil distribution in the Lower Hornerstown and Upper Navesink Formations at the Edelman Fossil Park, New Jersey: Frontiers in Earth Science, v. 9, 756655.
Wahyudi, H., 2010, Cretaceous-Paleogene transition on the New Jersey Coastal Plain: M.S. thesis, Rutgers University.
Yancey, T.E., and Guillemette, R.N., 2008, Carbonate accretionary lapilli in distal deposits of the Chicxulub impact event: Geological Society of America Bulletin, v. 120, no. 9-10, p. 1105-1118, https://doi.org/10.1130/B26146.1.
Zafar, M.N., Sabatier, P., Dutykh, D., Jomard, H., Rapuc, W., Lajeunesse, P., and Chapron, E., 2025, Modeling earthquake-induced seiche processes and subsequent homogenite deposition in lacustrine settings: Earth and Planetary Science Letters, v. 660, 119348.

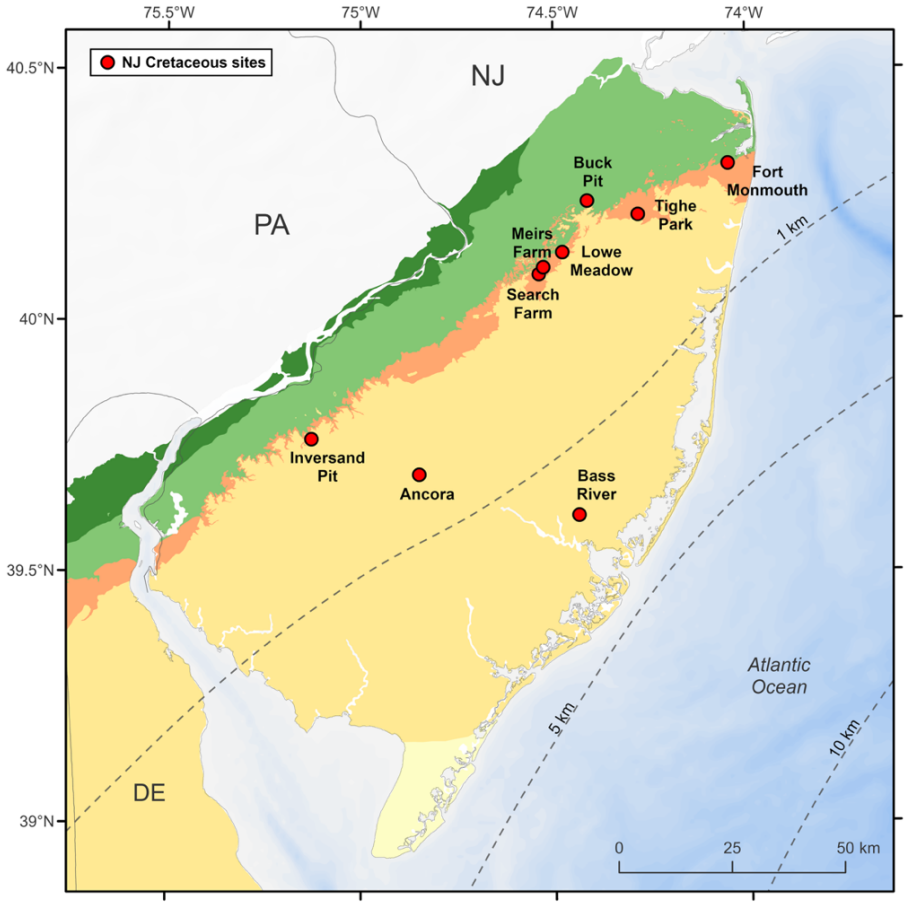


Figure 1. Location map showing sites (Inversand Pit is the current Edelman Fossil Park, Buck Pit is adjacent to Campo Pit). Dark Green in Lower Cretaceous; Light green is Upper Cretaceous; orange is Paleogene, dark yellow is Neogene, and light-yellow Quaternary. Dashed contours indicate depth to basement.

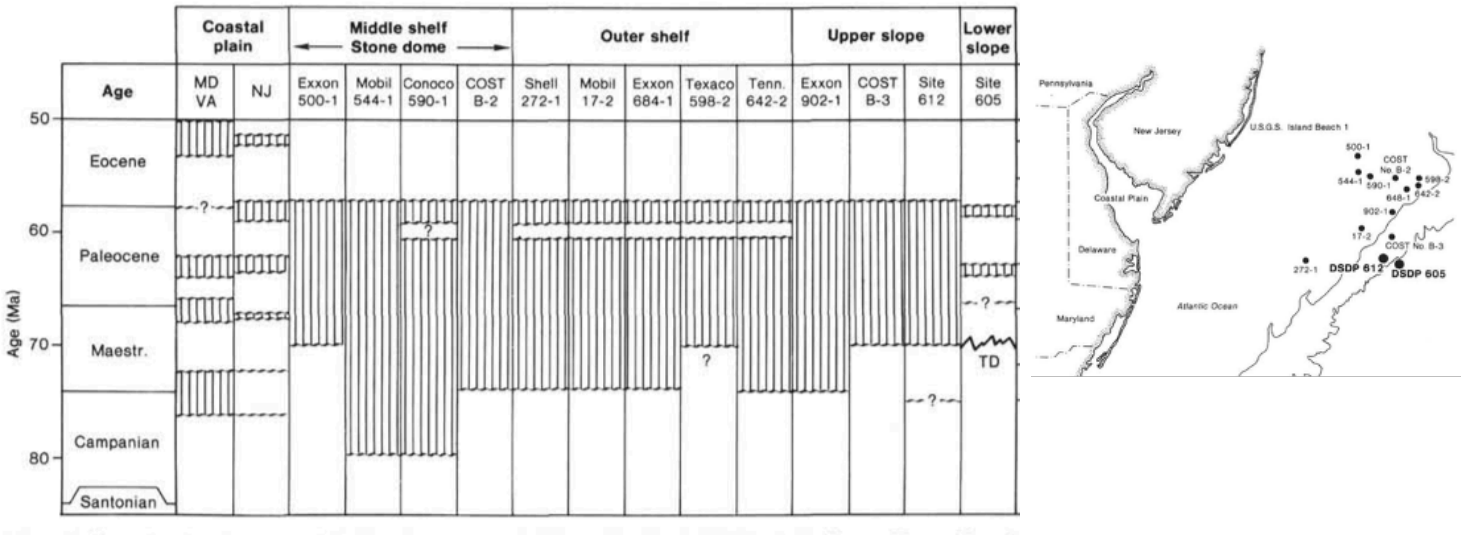


Figure 2. Data indicating the hiatuses of the East Coast Sequential Unconformity. From Olsson and Wise (1987).

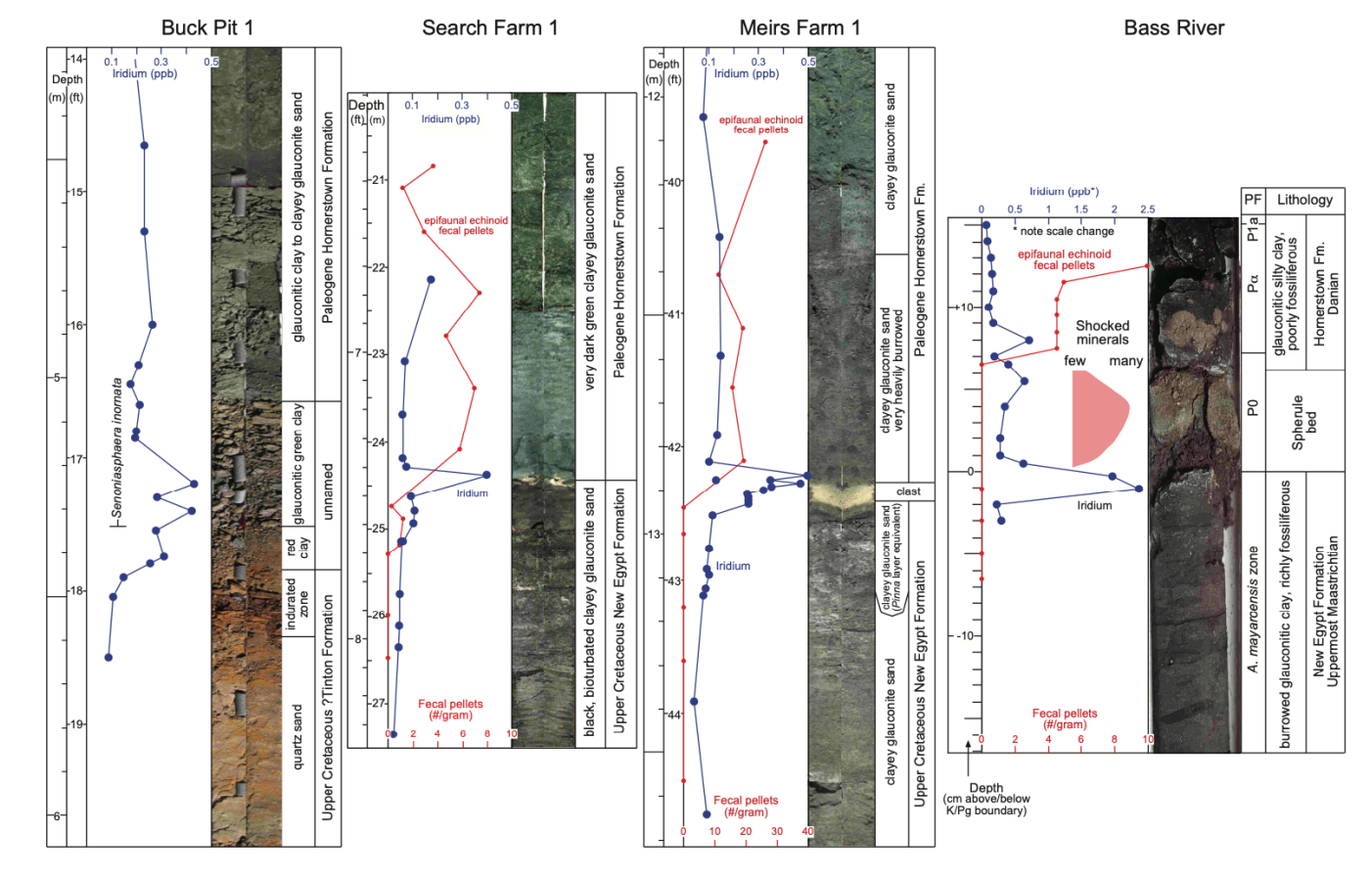


Figure 3. Core sections. Ir in parts per billion (ppb), fecal pellets in number/g of sediment, core photographs, lithology, and formational assignment for Buck Pit , Search Farm 1, and Meirs Farm 1 coreholes. Note that scale for Ir at Bass River (Olsson et al., 1997) is compressed relative to other locations. From Miller et al. (2010).

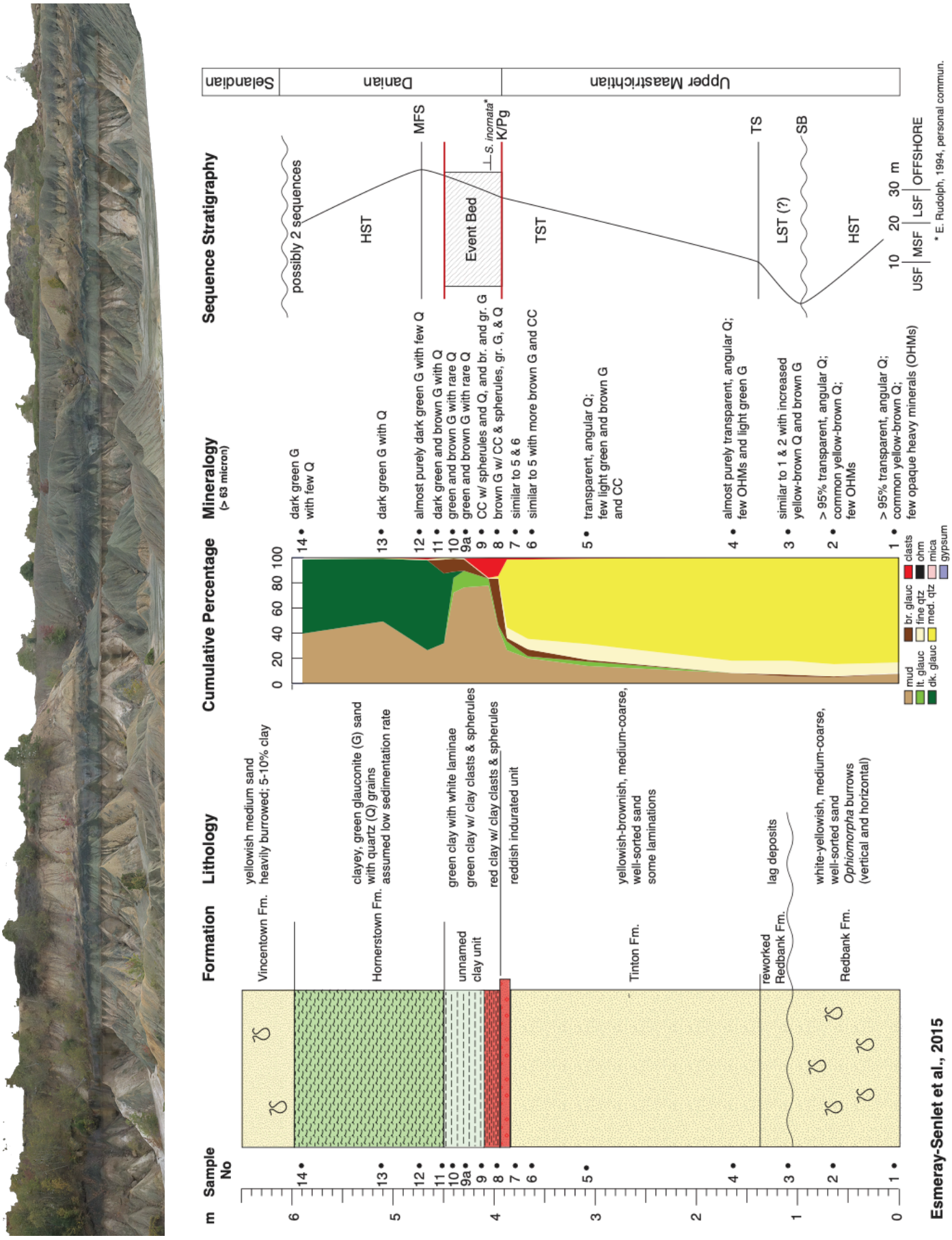


Figure 4A (top). Orthorectified composite drone imagery of the Campo Pit exposure in 2024; view of the image is ~180 m across.
Figure 4B (bottom). Sedimentology and stratigraphy across the K/Pg boundary in Campo Pit. Esmeray et al. (2015).







Figure 5a (top). HCS lower Shrewsbury Member, Campo-Buck Mining Pit, 2008

Figure 5b (middle). Swaley cross stratification, Campo-Buck Mining Pit, 2010

Figure 5c (bottom). Planar stratified upper shoreface deposits of the upper Shrewsbury Member, Campo Pit.

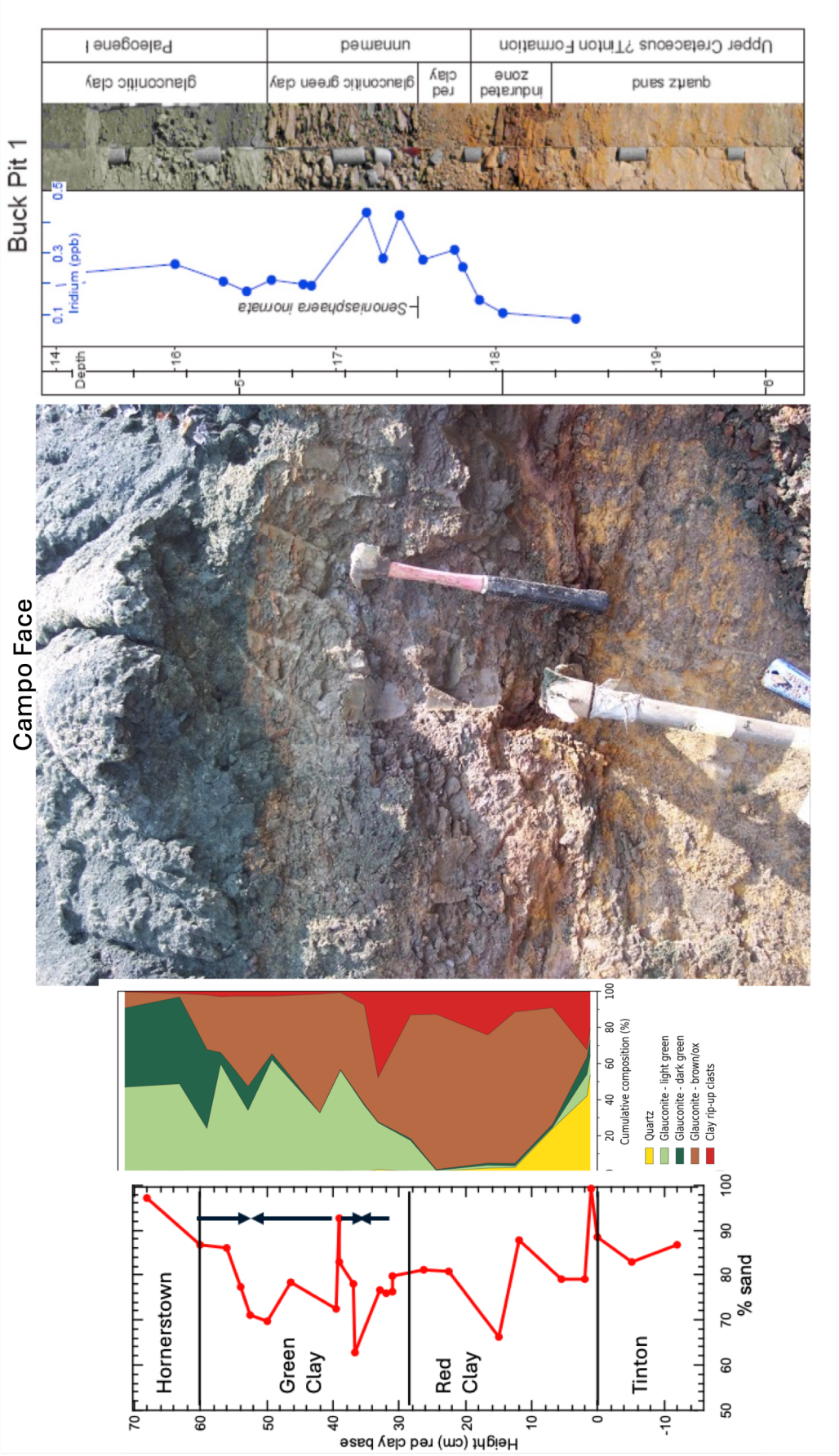


Figure 6. Campo percent sand, cumulative components, Campo outcrop photo (this study) correlated to Buck-1 core showing Ir concentrations (Miller et al., 2010).

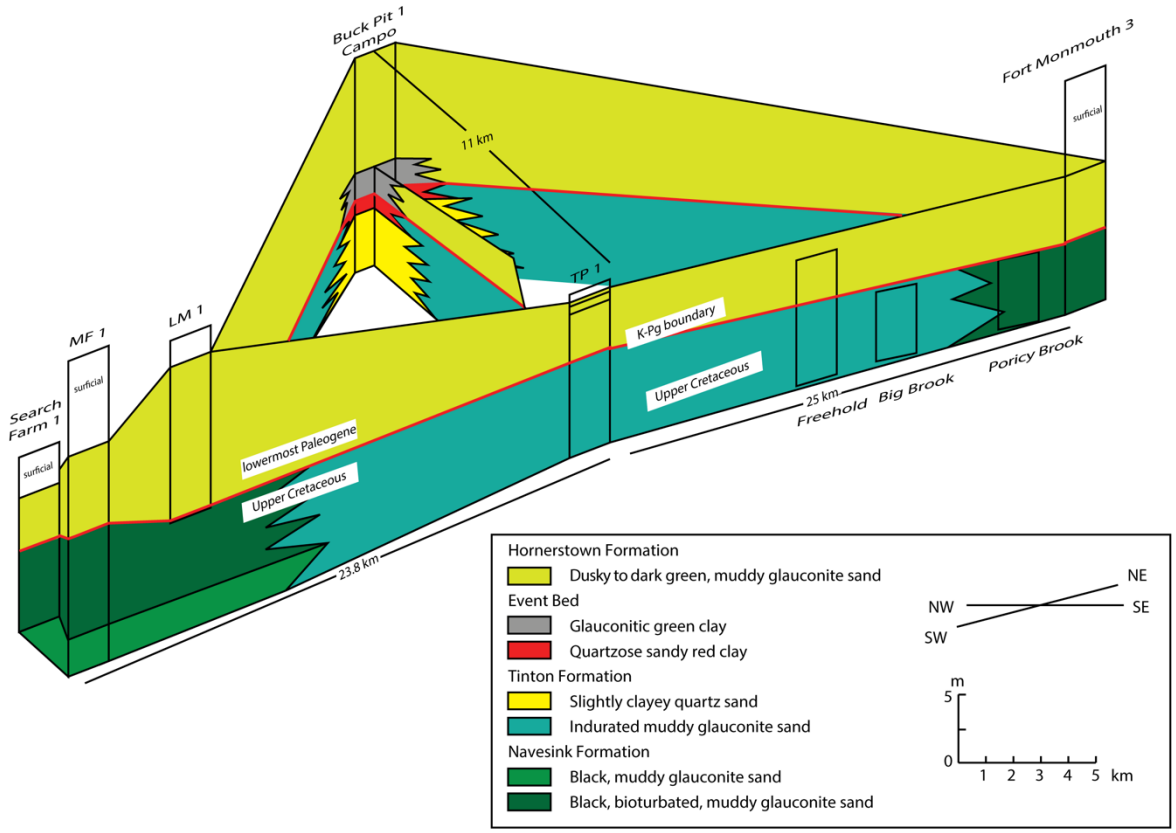


Figure 7. Fence diagram showing distribution of formations and facies in NW Monmouth County. Modified after Wahyudi (2010).



Figure 8a. Campo Pit, Feb. 2026. White layers at top of green clay. Photo by A. Hudak.



Figure 8b. Campo Pit, Feb. 2026. Load structure (load cast) transitioning to a ball-and-pillow pseudonodule produced by soft-sediment loading and liquefaction. Note numerous clay burrows in the yellow Tinton Formation below the Fe-cemented K/Pg boundary. Photo by A. Hudak.

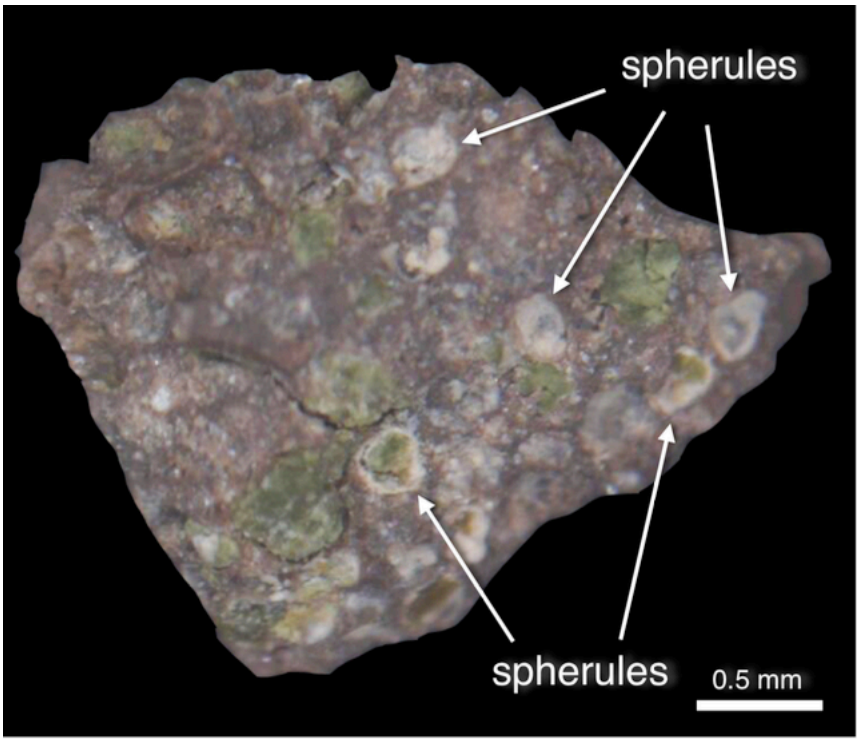


Figure 9a. Impact spherules found in the event bed above the K/Pg boundary in the green clay (sample 9, 4.1-4.5 m, Fig. 4). Scale bar represents 2 mm. From Esmeray-Senlet (2015).

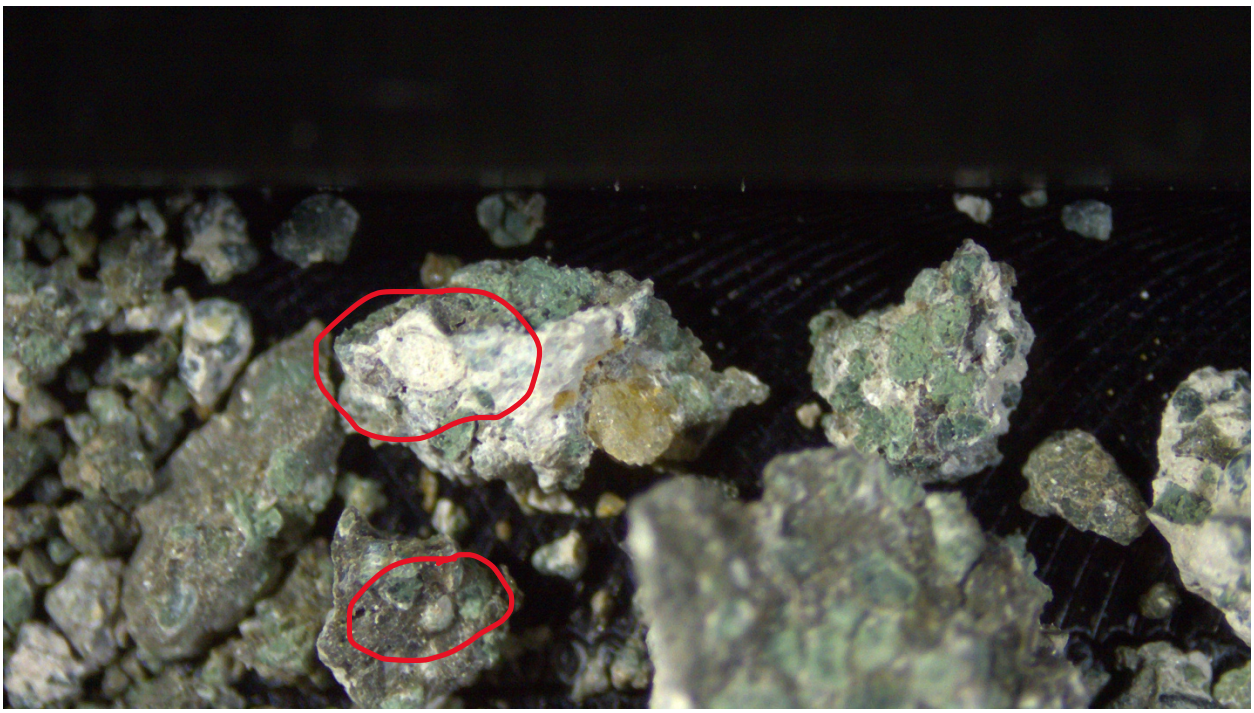


Figure 9b. Close up of a white lamina from Campo Pit showing the kaolinite-rich clay cement. grains. Possible spherules bottom circle, possible spherule impression top circle. Photo by A. Hudak.



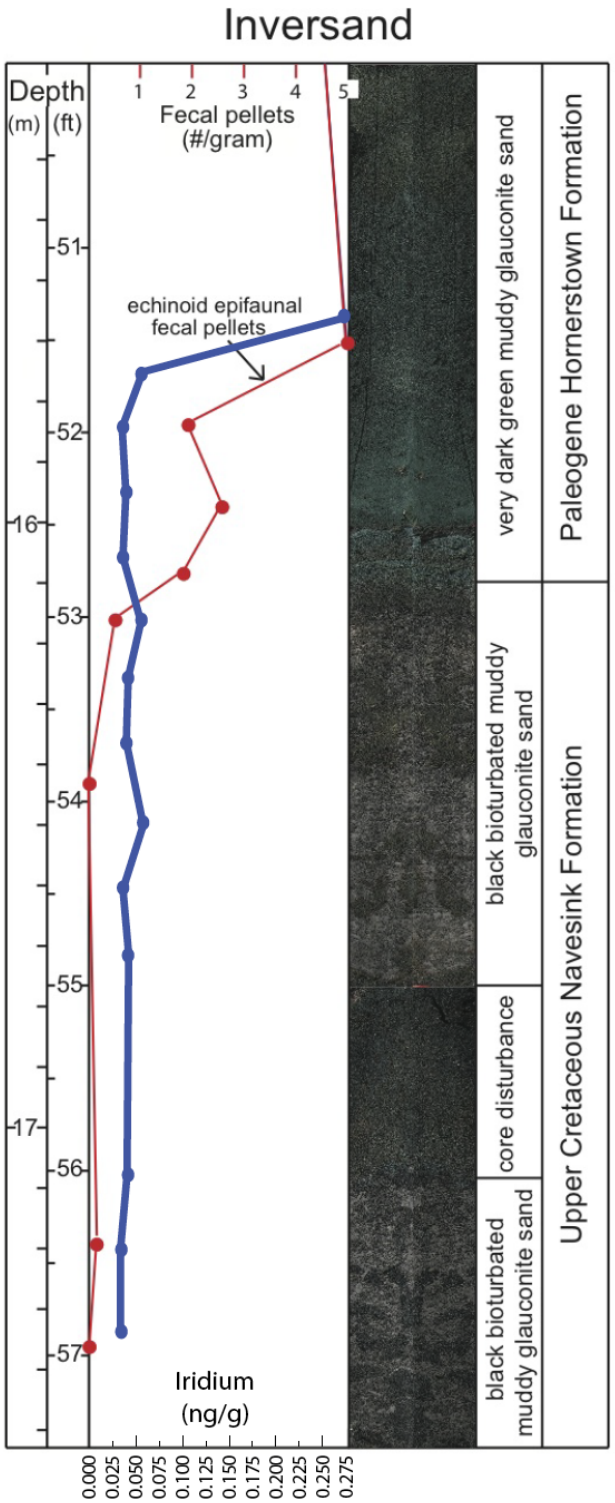


Figure 10. Photo from the Inversand Pit (now Edelman Fossil Park) showing contact of the Navesink brown clays with the burrowed Hornerstown Formation at the level of the micropick. The main fossiliferous layer is at the top of the tape measure. Ir was measured on the adjacent Inverand 1 core. The lower increase in echinoid fecal pellets (red) marks the K/Pg. Core data from the adjacent Inversand core Esmeray-Senlet et al. (2015)

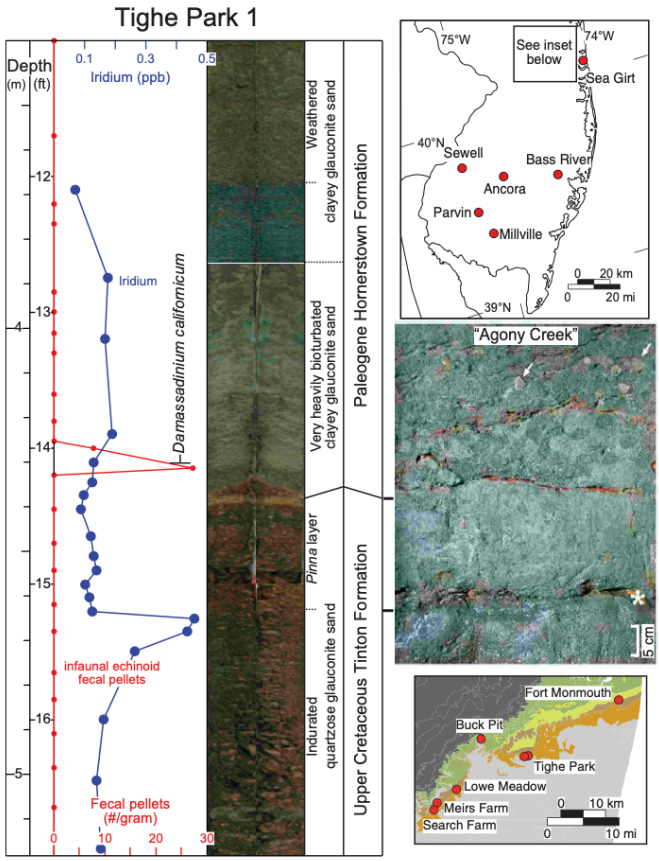


Figure 11. Freehold, New Jersey, sections. Ir in parts per billion (ppb), fecal pellets in number/g of sediment, core photographs, lithology, and formational assignment for Tighe Park 1 corehole. First occurrence of Danian dinocyst index fossil *Damassadinium californicum* is after Landman et al. (2007). Also shown is outcrop photograph from Landman et al. (2007) from an adjacent (~190 m east) tributary ("Agony Creek") of Manasquan River. Asterisk indicates level of Ir anomaly in this section. Inset location map shows outcrop of post-Campanian Cretaceous (dark-green Red Bank and light-green Tinton Formations) and Paleocene (brown Hornerstown and mustard/yellow Vincentown Formations) strata; pre-Maastrichtian strata are in dark gray; post-Paleocene strata are light gray. From Miller et al. (2010).

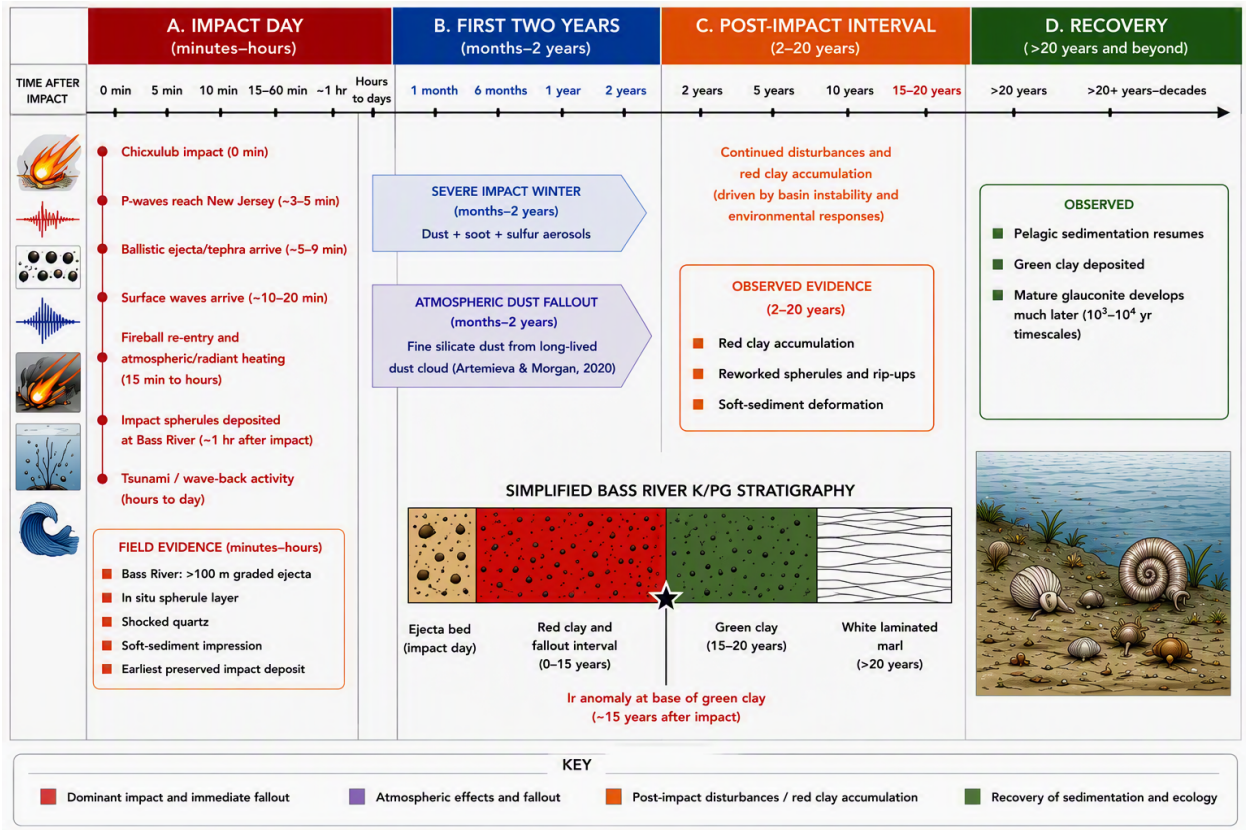


Figure 12. Proposed Chronology of the Chicxulub Impact in the New Jersey Coastal Plain. Figure was drafted with the assistance of Microsoft Copilot AI.

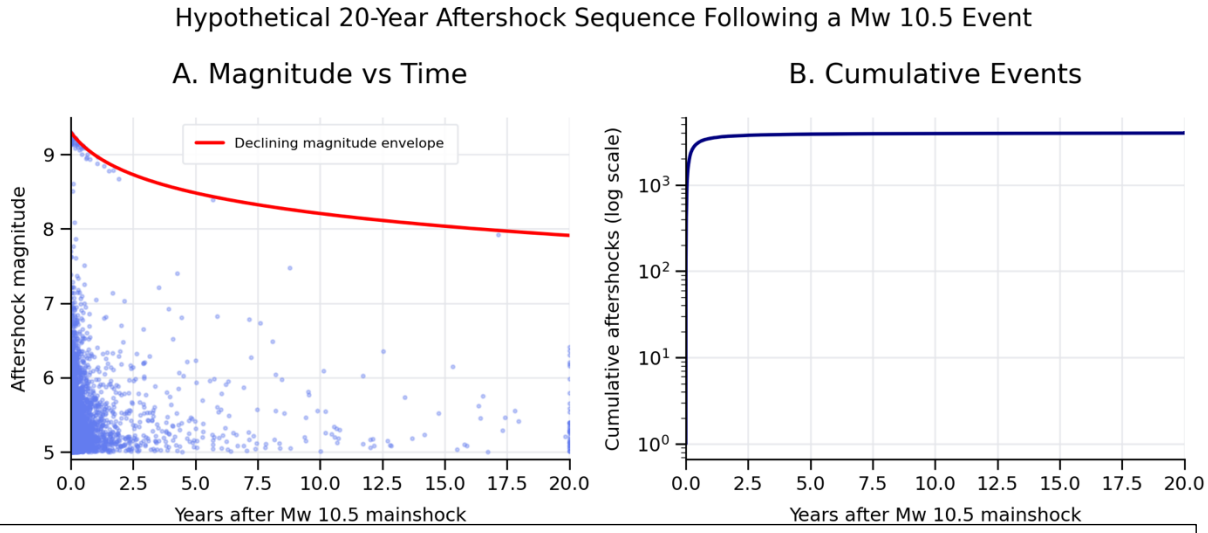


Figure 13. Hypothetical aftershock evolution following a Chicxulub-generated Mw 10.5 seismic event. (A) Simulated aftershock magnitudes plotted against time since the impact-generated mainshock. Red curve shows a declining upper-magnitude envelope extrapolated from Bath's Law and observations of long-lived aftershock sequences. (B) Corresponding cumulative number of aftershocks calculated using an Omori-type decay relationship. Most aftershocks occur within the first several years, but large earthquakes (Mw > 8) remain possible throughout much of the first decade, with Mw 7-8 events potentially persisting for two decades. Magnitude and frequency distributions beyond the range of observed terrestrial earthquakes should be viewed as heuristic extrapolations rather than predictive models. Figure was drafted with the assistance of Microsoft Copilot AI.

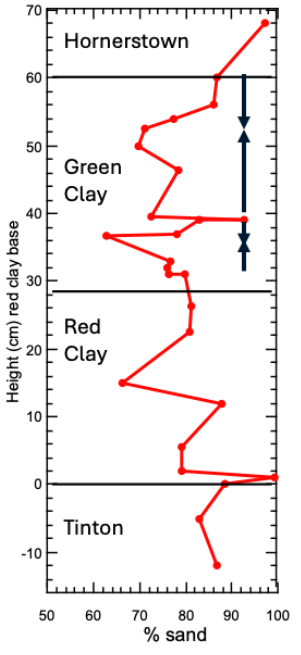
SUPPLEMENTARY MATERIAL

Grain Size Data

Twenty-six samples were collected from the South Outcrop at Campo in 2026, near the northernmost appearance of trees ("Last Tree Outcrop"; ~ 40°14'6.15"N; 74°24'43.33"W). Samples were taken every 2–3 cm with a hand auger extending 2–10 cm into the face, disaggregated in Calgon, and wet sieved through a 63 µm mesh. The samples from Indurated zone, red Clay, and green clay contained indurated fragments that did not completely break down during processing. These resistant fragments occurred in both the red and green clay units and may affect coarse fraction grain-size distributions reported here.

Grain-size analysis indicates that the section is sand-rich. Sand percentages range from 63% to 99%, with a mean sand content of 80.6% (n = 26). The highest sand contents occur within the Tinton and Hornerstown Formations, whereas lower values characterize the red and green clay units, where much of the sand sized particles consist of reworked clasts.

Representative grain-size analyses were obtained using a Horiba LA-950 laser particle-size analyzer from (1) the middle (approximately Sample A9 in Figure 4) and (2) a white lamina near the top of the clay interval. The results



Height cm	relative to base Red Clay cm	Unit	Sample	% sand
89	-12	Tinton	A-2	86.8
96	-5	Tinton- below	A-1	82.8
101	0	Red Clay Bas	A1	88.6
102	1	Tinton	A0	99.4
103	2	Red Clay -Re	A1.1	79.1
106.5	5.5	Red Clay	A2	79.2
113	12	Red Clay	A3	87.9
116	15	Red Clay	A4	66.1
123.5	22.5	Red Clay	A5	81
127.25	26.25	Red Clay	A6	81.2
128	31	Green Clay	A7	79.8
132	31	Clay Unit	B2	76.4
132	32	Clay Unit	B3	76
133	33	Green Clay	A8	76.7
134	36.7	Green Clay	A9	62.8
137.7	37	Clay Unit	B4	77.9
140	39	Clay Unit	B1	82.8
140	39	Clay Unit	B1.1	92.8
140.5	39.5	Green Clay	A10	72.6
147.5	46.5	Clay Layer- N	A11	78.3
151	50	Clay Unit	A12	69.7
153.5	52.5	Clay Unit- Ne	A13	71
155	54	Clay Unit- Lo	A14	77.2
157	56	Clay Unit- Up	A15	86.2
161	60	Hornerstown	A16	86.7
169	68	Hornerstown	A17	97.2

part of the green clay unit

Figure S1, Table S1. percent sand versus stratigraphic position relative to the base of the red clay unit. Arrows point in fining direction.

indicate that both samples contain substantial silt and very fine sand, but the white lamina is distinctly finer grained than the underlying green clay sample.

The green clay sample displays a dominant peak at approximately 72 µm (very fine sand; mode = 72.4 µm) and a secondary peak centered near 12-16 µm (medium to coarse silt). The finer mode represents a substantial silt population, whereas the coarser mode corresponds to very fine sand. The bimodal distribution suggests mixing between a suspension-settled silt fraction and a higher-energy very fine sand fraction. The median grain size is 41.5 µm, reflecting the influence of both particle populations.

The white lamina sample exhibits a more complex, trimodal distribution. Peaks occur at approximately 0.3-0.4 µm (clay to colloidal fraction), 10-15 µm (fine to medium silt), and 80-90 µm (very fine sand; mode = 82.6 µm). Although the coarsest peak is the strongest, the distribution contains a much larger proportion of fine-grained material than the green clay sample, resulting in a substantially finer median grain size of 22.9 µm. The presence of three distinct populations suggests deposition from multiple transport mechanisms or hydraulic regimes, possibly involving background suspension settling, fine-silt influx, and episodic delivery of very fine sand.

These multimodal distributions indicate that neither unit is composed of homogeneous clay. Instead, the green clay consists primarily of mixed coarse silt and very fine sand populations, while the white lamina contains distinct clay-, silt-, and sand-sized components. The finer median grain size and stronger fine-grained modes in the white lamina suggest a reduction in depositional energy relative to the underlying green clay, although both samples retain an appreciable very fine sand component.

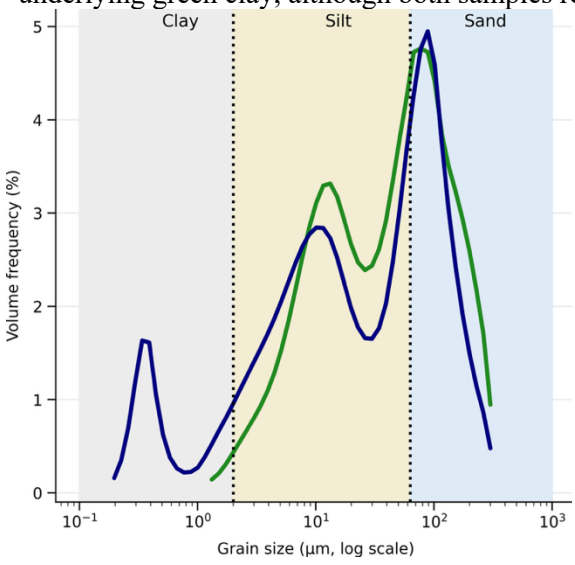


Figure S2. Grain-size distributions determined by Horiba LA-950 laser diffraction analysis for ultrasonicated samples from the middle green clay unit (green line) and an upper white lamina (purple line) at Campo. The green clay sample exhibits a bimodal distribution with modes at 10.8 and 82.8 µm; the white lamina displays a trimodal distribution consisting of clay-sized (<1 µm), silt-sized (~12 µm), and very-fine-sand-sized (~83 µm) populations. Both share a prominent very-fine-sand mode near 83 µm, suggesting a common coarse sediment component. Vertical dashed lines denote the clay-silt (2 µm) and silt-sand (63 µm) boundaries. The finer D50 and additional clay-sized population in the white lamina indicate greater preservation or input of fine-grained material relative to the green clay. Figure prepared by recovering and reanalyzing legacy grain-size data using Microsoft Copilot AI.

Clay Mineralogy Studies

Background information

Kaolinite and chlorite can be difficult to distinguish by X-ray diffraction because both have a strong peak near 12.5° 2θ and closely spaced peaks near 25° 2θ. Heating to 550°C provides a diagnostic test: kaolinite becomes amorphous and its peaks collapse, whereas chlorite peaks persist, although they weaken and shift slightly. Glauconite and illite also show similar diffraction patterns, sharing peaks near 8.8, 17.8, 19.8, and 26.7° 2θ. Illite peaks are typically sharp and symmetrical, whereas glauconite peaks are broader and more diffuse. After heating to 550°C, illite remains largely unchanged, while glauconite peaks become sharper and better defined.

Methodology

X-ray diffraction (XRD) data of the white layer were collected on a Philips XPERT Powder Diffractometer at Rutgers University. Samples were prepared as described by Poppe et al., 2001 and Moore and Reynolds, 1997. Untreated sample data were collected with a scan range of 5 to 50° 2θ using a step size of 0.04 for 3 seconds per step. The sample was then placed in a muffle furnace and heated at 550°C for two hours. The heated sample data were collected with a scan range of 3 to 30° 2θ using a step size of 0.02 for 3 seconds per step. Peak fitting and phase identification was performed using Panalytical HighScore Plus.

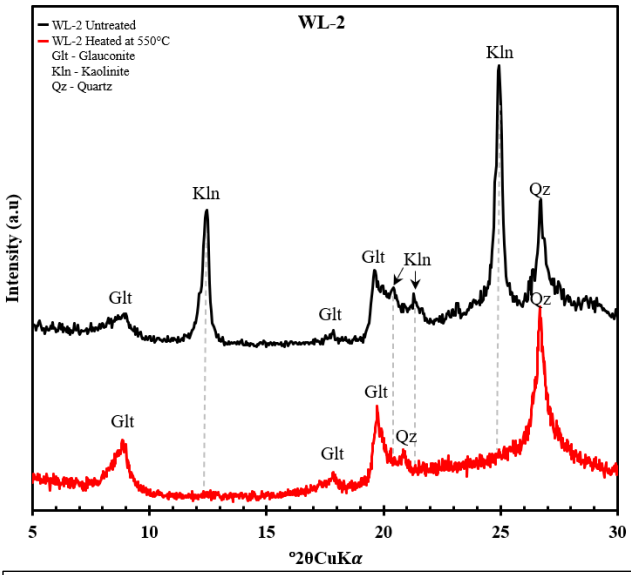


Figure S3 X-ray diffraction (XRD) pattern of white-layer sample WL-2. XRD patterns of the untreated sample (black) and the sample heated to 550°C (red). Gray dashed lines indicate kaolinite peaks that collapsed after heating, confirming the presence of kaolinite and absence of chlorite in the sample.

Results

The XRD pattern of the untreated white-layer sample displayed peaks characteristic of kaolinite and/or chlorite, quartz, glauconite, and illite. After heat treatment at 550°C, the kaolinite peaks decomposed. If chlorite were present in this sample, diffraction peaks would have remained at 12.5 and ~25° 2θ. The lack of defined peaks at these angles indicates that chlorite is absent and kaolinite is present. The broad asymmetrical peaks at 8.8, 17.8, and 19.8° 2θ in both diffractograms suggest glauconite over illite.